XIII International Conference on Computational Plasticity. Fundamentals and Applications
COMPLAS XIII
E. Oñate, D.R.J. Owen, D. Peric and M. Chiumenti (Eds)

NUMERICAL STUDY OF CONDITIONS FOR SUBSURFACE SHEAR INSTABILITY UNDER CONTACT INTERACTION

ANDREY I. DMITRIEV[*,†,‡], VIKTOR P. KUZNETSOV[‡‡] AND SERGEY YU. TARASOV[*,‡]

[*]Institute of Strength Physics and Materials Science (ISPMS), Russian Academy of Science
Akademichesky pr. 2/4, 634021 Tomsk, Russia
e-mail: dmitr@ispms.tsc.ru, web page: http://www.ispms.ru/

[†]National Research Tomsk State University (TSU)
Lenin pr. 36, 634050 Tomsk, Russia
web page: http://www.tsu.ru

[‡]National Research Tomsk Polytechnic University (TPU)
Lenin pr. 30, 634050 Tomsk, Russia
web page: http://www.tpu.ru

[‡‡]Ural Federal University, Ekaterinburg, Russia (UrFU)
Mira street 19, 620002 Ekaterinburg, Russia
web page: http://www.urfu.ru

Key words: numerical modeling, movable cellular automata, nanostructuring, burnishing, shear instability.

Abstract. Numerical modeling of nanostructuring burnishing has been carried out to reveal the limiting values of process parameters, which serve both to provide the appropriate surface quality and positive deformation-induced structural modification of the subsurface layers as well as to avoid shear instability in the subsurface layers of burnished metal. The effects of load, burnishing speed, tool pass number and tribological transfer on the burnished surface roughness have been elucidated by the example of quenched and tempered steels 20X (EN 20Cr4). It was shown that overloading results in quasi-viscous flow of the subsurface material, deterioration of the surface and ruining the positive effect of nanostructuring burnishing.

1 INTRODUCTION

It has been shown in [1] that combination of normal and shear plastic strain induced in sliding provides severe plastic deformation and fast generation of a nanosize subgrain layer in the subsurface of metals in sliding which may lead to shear instability of this layer with respect to shear stress. The origin of such phenomenon is related to changing the deformation

mechanism at the real contact areas from shear to grain boundary slipping in nanosize SPD-generated structures. This structurally modified and plasticized material is deformed as a quasi-viscous medium and has very strong adhesion to the counterpart thus causing galling and seizure. It is plain to see that the processed surface's quality may serve as an indicator to notice the shear instability onset which normally has to be avoided when presenting the burnishing process parameters. Another part of the story is that nanosize subgrains generated by sliding in the subsurface provide hardening due to Hall–Petch law and thus may reduce the wear rate of the component processed. So the choice is to generate the optimum thickness nanosize subgrain structure but avoid its instability against shear stress in the subsurface of metals.

The objective of this work is to establish the limiting nanostructuring burnishing process parameters by the criterion of shear instability onset in the subsurface material layer and workpiece-to-tool metal transfer. To achieve this, the numerical modelling of the nanostructuring burnishing process was undertaken. The subsurface structural modification is determined by the power of the friction process, i.e. the energy delivered to the subsurface per time. Numerical modelling was devoted to studying the effect of loading and number of passes on the subsurface structural modification.

2 MATERIALS AND METHODS

Steel samples have been fabricated of steel 20X (EN 20Cr4) (see Table 1) in the shape of 80 mm diameter, 12 mm thickness disks. Steel samples have been carburized by gas to obtain 0.95 wt. % concentration of carbon at the 0.1 mm depth below the surface. The final heat treatment was quenching 839°C in oil and tempering 250°C for 2 hr. The amount of retained austenite was 30 vol. %. The hardness of the sample was HRC55.

Table 1: Chemical composition of steel 20X

	Composition, wt.%							
Element	C	Cr	Ni	Mn	Si	Cu	P	S
20X	0.21	0.84	0.08	0.57	0.27	0.18	0.017	0.019

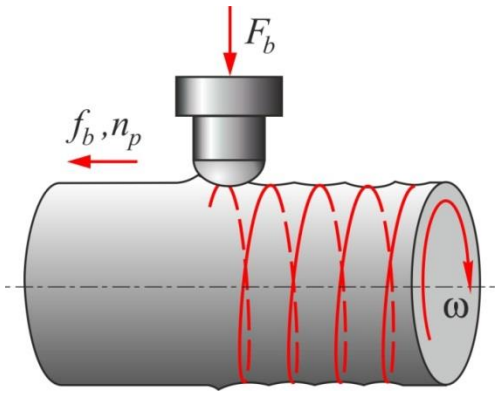

Figure 1: Schematics of the nanostructuring burnishing by half-spherical indenter's tip of radius R. F_b – normal load; ω – rotation rate correlated with burnishing rate v_b, f_b – feed, n_p – tool pass number.

Before nanostructuring burnishing, the samples have been precision turned by Sandvik WNGA 08048 hard metal cutters at cutting speed v_c=80 m/min and feed rate $S_т$=0.06 mm/rev for one tool setting block on Multus B300-W turning and milling center. The surface roughness was 0.34 μm. The nanostructuring burnishing of the 20X(HRC55) steel has been carried out using R=2 mm spherical tool of polycrystalline DBN material as schematically shown in Fig.1 and corresponding friction coefficients were μ=0.34 and μ=0.13 for dry sliding conditions and lubrication by Rhenus coolant, respectively. The normal load F_b was 200 N, feed rate f_b=0.04 m/rev.

The microstructure of the samples have been examined using TEM instrument JEOL JEM-2100, SEM instrument Tescan Mira 3 LMU with autoemission Schottky cathode and scanning autoemission electron microscope AURIGA CrossBeam. Surface roughness was determined using optical profilometer Wyko NT-1100.

3 EXPERIMENTAL RESULTS

The nanostructuring burnishing was under conditions F_b=200, 400 and 600 N; μ=0.34; feed rate S_b=0.04 mm/rev; f_b=10 m/min; n_p=4. The subsurface structure of the samples after nanostucturing burnishing has been modified so that the martensite needles were replaced for superfine deformation-induced structures.

The intensity of subsurface deformation in burnishing depends on the normal load value. The SEM images in Fig. 1 for a single tool pass show us the burnished surfaces obtained at different normal load values. We can see almost smooth surface with some grooves for F_b =400 N (Fig. 2a) and totally deteriorated surface for F_b =600 N (Fig. 2b). Too high normal load and, correspondingly, the friction force induces the shear instability which results in quasi-viscous flow and discontinuities of severely deformed subsurface layer thus giving us the same burnished surface pattern as seen in Fig. 2b, where such an effect has been achieved by strain accumulated at lower normal load but higher tool pass number.

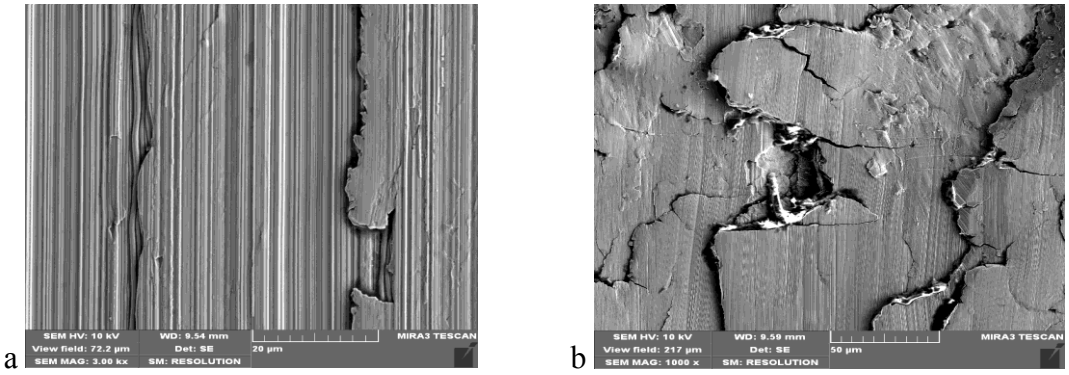

Figure 2: The SEM images of 20X steel surfaces burnished at (a) F_b =400 and (b) F_b =600 N

4 NUMERICAL MODELING OF THE NANOSTRUCTURING BURNISHING

4.1 The model description

For numerical modeling the method of movable cellular automata (MCA) was used. The

general concept of the MCA method is an extension of conventional cellular automaton approach by incorporating some basic postulates and relations of particle-based methods [2]. The movable cellular automaton is an object of finite size, possessing translation and rotation degrees of freedom. The concept of MCA method is based on the introduction of a new type of state, namely the state of a pair of automata (elements). In the considered case there are two types of pairs of automata: chemically bonded (named as "linked") and "unlinked". According to [3] the transition from the first to second allows one to simulate the damage of the material. Also Österle in [4] reported that the transition of an automata pair from linked to an unlinked state (which is physically interpreted as fracture with subdivision of the pair into two independent automata) changes the character of their interaction. The principles of putting down the equation of motion for a system of movable cellular automata and prescribing interactions between them have been presented in [3, 5]. In [6] was stated that in contrast, for example, to the method of discrete elements, the MCA method uses the many-particle interaction where the force calculation is based on the spatial configuration of nearest neighbors.

For numerical movable cellular automata modeling we have chosen a contact zone spot between two bodies in sliding with relative velocity transversely directed with respect to compressive stress as shown in Fig. 3.

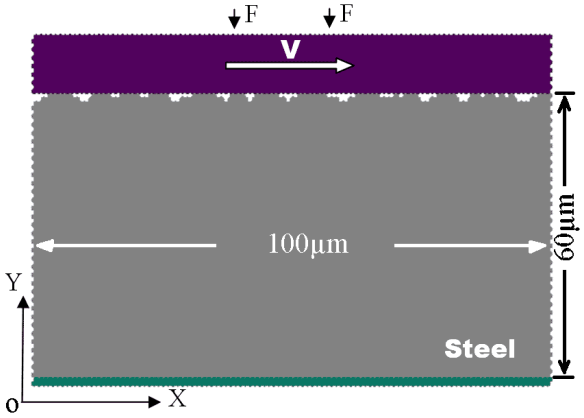

Figure 3: The structure of the modeled setup and a scheme of loading

The model included two blocks belonging to the bodied in sliding contact. The upper block was an indenter, while the lower one played a role of the steel to be burnished. The automatons of upper block have been loaded by external force which induced 1 to 10 MPa stresses directed along the OY axis. On establishing the equilibrium, a transversal driving force has been applied in the direction of OX to move the upper block at V=0.5 m/s. The positions of the lower block automatons have been fixed to simulate the elastic response of the burnished material. The loading parameters have been specified by doing so and then corresponded to severe and confined conditions of the sliding contact. In order to exclude the influence of the edge effects we imposed periodical boundary conditions along the OX axis, which simulated the dimension of the "assembly" generated. The length of the zone of interest was 0.1 mm for the automaton size as small as 1 μm. The number of automatons in the modeled fragment was above 9000. The physical characteristics of the indenter's and

sample's automatons corresponded to those of superhard material and quenched to HB ≥ 340…400 steel, respectively. The properties defining the stress-strain responses of the modeled materials are listed in Table 2. The initial roughness of the contacting surfaces has been simulated by pulling some automatons out of the superficial layer.

Table 2: Mechanical properties of the modeled materials

Property	Steel	Indenter
Young's modulus, GPa	206	1140
Poisson's ratio	0.28	0.07
Elastic limit, MPa	520	13500
Yield strength, MPa	800	13700
Tensile strength, MPa	920	14000
Strain at yield strength	0.04	0.012
Strain until fracture	0.106	0.013

4.2 Results of modeling

Our computations demonstrate that on being brought in sliding contact, the asperities immediately start deforming and fracturing. Simultaneously, new linked pairs are created so that the result is the generation of a structurally modified subsurface layer under the loading. This structural modification penetrates only to 5 – 8 μm depth below the surface unless corresponding normal stress is higher than 5 MPa. The steady-state configurations of the inter-automaton ties are shown in (Fig. 4a) where the linked pairs correspond to no-modification states and are marked by lines connecting the relevant automatons' center points. It can be seen that the zone where automata pair state switching occurs stays localized within the indenter/sample contact area for all time intervals. Similar conclusion is feasible from the analysis of the strain intensity fields (Fig. 4b) obtained for the same moment of time. The strain intensity is higher at the areas where the best mating condition between the indenter and sample surfaces are provided. This, however, does not cause increasing the thickness of the subsurface layer with maximum strain intensity for the time interval given.

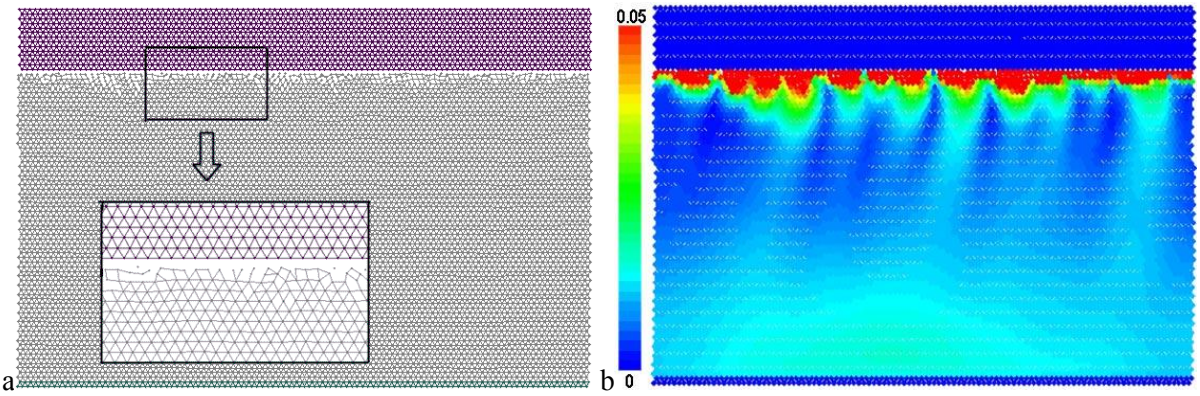

Figure 4: The evolution of inter-automata ties (a) and strain intensity distribution (b) for moment of time $t=1.5\cdot10^{6}\Delta t$.

Increasing the compressive stress up to 6 MPa and even higher corresponds to applying the indenter of radius 2 mm and burnishing force $F_b \geq 200$ N thus serving to intensify the subsurface structural modification. Structural evolution of the inter-automaton ties as well as strain intensity field for compressive stress level as high as 8 MPa is shown in Fig. 5 where it can be seen that the thickness of the layer with broken inter-automaton ties is more than 10 μm. According to Fig. 5a it is possible to distinguish two types of layers by typical structure of ties between the particles. The top 10 μm thickness layer is in direct contacting with the indenter and here we can see its active structural modification. The interparticle ties are being broken and restored in this layer thus serving to develop processes of segmentation and intermixing. As before, the thickness of the layer is kept constant for the steady state motion.

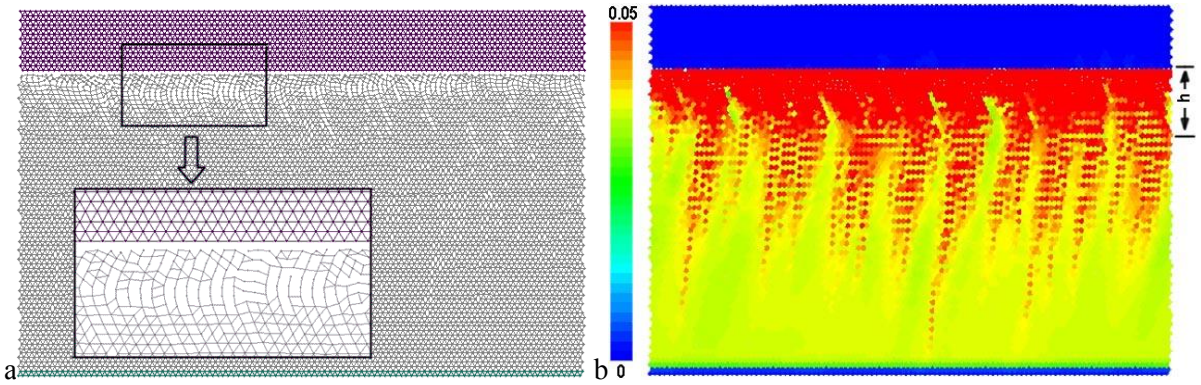

Figure 5: The evolution of inter-automata ties (a) strain intensity distribution (b) for moment of time $t=1.5 \cdot 10^6 \Delta t$. h is the thickness of the layer with broken automata ties.

The distribution of strain intensity values reconstructed for the one and same moment of time also indicates on higher intensity and strain penetration depth in the subsurface of the material (Fig. 5b). The layer's thickness may be estimated by a magnitude of high strain intensity effective bending. The arrow shows a position of structural bending.

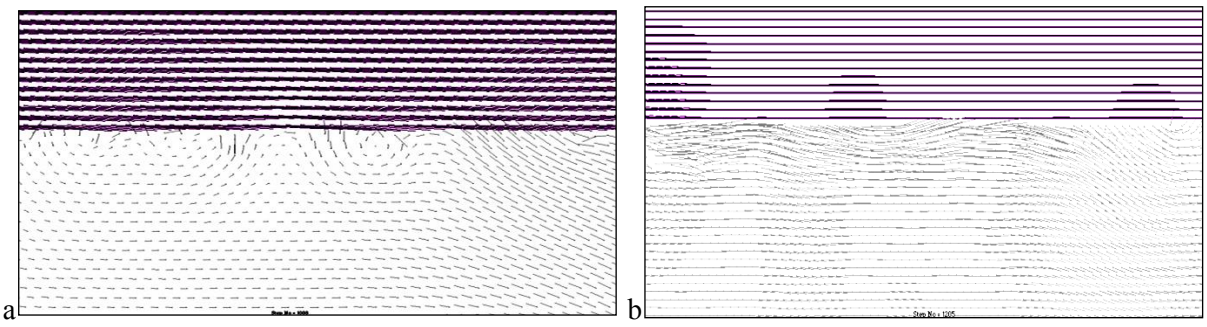

Figure 6: Fields of particle velocity near the specimen surface for two different moments of time

The particle velocity field for a part of the sample below the free surface is shown in Fig. 6 for moments of time $t=1.108 \cdot 10^6 \Delta t$ and $t=1.205 \cdot 10^6 \Delta t$. In contrast to the sliding regime shown on the Fig. 6a the velocity field on the Fig. 6b demonstrates us complex and non-linear

behavior of the particles' motion in the vicinity of indenter/sample contract area. Such a mode of motion could be even called a “quasi-viscous” flow mode, which is a signature of shear instability in metals as demonstrated in [7].

Let us note that according to Fig. 5a, the interautomaton tie breakdown criteria may be achieved even below the top subsurface layer but no intermixing action is observed. The strain intensity field shows up here as a homogeneous one.

5 DISCUSSION

By modeling the effect of burnishing by a superhard indenter on subsurface deformation in sliding steel sample we found two different deformation modes which differ from each other by the strain intensity penetration depth and material flow pattern. The first mode is observed for compressive stress 1 to 5 MPa and characterized by the strain penetration depth in the range 5 to 8 μm. The second mode shows total strain penetration to more than 10 μm below the surface at compressive strength 8 MPa with first 10 μm of material being dragged and stirred by the indentor. The behavior of material particles in this layer is very similar to that of observed during sliding with seizure when a plasticized metal layer flows like a quasi-viscous nanocrystalline material under condition of shear instability [8]. In spite of the fact that such a treatment serves to produce nanosized subgrain structure and thus increase the hardness, the quasi-viscous flow would strongly affect the surface quality. Therefore, it would be a wise decision to avoid applying loading condition that lead to establishing such a mode.

In so doing, numerical simulation shows that overloading in burnishing results in structural changes the intensity of which depends on the strain degree and strain penetration below the surface. Two structurally different layers have been observed in numerical burnishing experiment as follows: (i) high strain layer of non-linear particle motion behaviour or quasi-viscous flow and intermixing mode and (ii) underlying layer of less strain degree showing only the plastic deformation (broken ties) but no intermixing.

Physical modeling the behavior of subsurface metal under burnishing conditions deals with higher number of external and internal factors contributing to the process such as load, speed, friction coefficient, number of tool passes, temperature, adhesion, etc. Nevertheless, numerical modeling is capable of distinguishing between two modes of the material behavior during burnishing.

6 CONCLUSION

- Overloading conditions in burnishing result in generation of a subsurface layer of non-linear quasi-viscous behavior. The origin of layer is similar with that of nanocrystalline layer obtained in tribological experiments under conditions of shear instability and intermixing and therefore could be called a tribological layer.
- There is a consistency between the results of numerical and physical modeling in the sense of generation of shear instability motion in the subsurface of the steel in burnishing.

Acknowledgements:
This work was partly supported by RFBR grant no. 15-08-01511-a. A.I.D. is grateful to acknowledge financial support from the Russian Science Foundation grant 14-19-00718.

Furthermore, the authors would like to acknowledge the Tomsk State University Academic D.I. Mendeleev Fund Program in 2014- 2015.

REFERENCES

[1] Tarasov, S.Yu., Lychagin, D.V., Chumaevski, A.V. Orientation dependence of subsurface deformation in dry sliding wear of Cu single crystals. *Appl. Surf. Sci.,* (2013) **274C**:22-26.
[2] Pöschel, T. and Schwager, T. *Computational granular dynamics*, Springer-Verlag Berlin Heidelberg (2005).
[3] Psakhie, S.G., Shilko, E.V., Smolin, A.Yu., et al. Approach to simulation of deformation and fracture of hierarchically organized heterogeneous media, including contrast media1. *Phys. Mesomech.,* (2011) **14(5-6)**:224-248.
[4] Österle, W., Dmitriev, A.I., Kloß, H. Does ultra-mild wear play any role in dry friction applications, such as automotive braking? *Faraday Discuss.,* (2012) **156**:159-171.
[5] Psakhie, S.G., Horie, Y., Ostermeyer, G.P., et al. Movable cellular automata method for simulating materials with mesostructure. *Theor. Appl. Fract. Mech.* (2001) **37**:311-334.
[6] Dmitriev, A.I., Österle, W. Modeling the sliding behavior of tribofilms forming during automotive braking: Impact of loading parameters and property range of constituents. *Tribol. Lett.* (2014) **53**:337–351.
[7] Dmitriev, A.I., Schargott, M., Popov, V.L. Direct modeling of surface topography development in a micro-contact with the movable cellular automata method. *Wear* (2010) **268 (7–8)**:877-885.
[8] Tarasov, S.Yu., Rubtsov, V.E. Shear instability in the subsurface layer of a material in friction. *Phys. Solid State* (2011) **53(2)**:358-362.